JOURNAL OF CATALYSIS **163,** 204–214 (1996)
ARTICLE NO. 0320

An XPS, TEM, and TPD Study of the Oxidation and Ammoxidation of Propene Using Mixed Fe–Sb Oxide Catalysts

Matthew D. Allen,* Stephen Poulston,* Erica G. Bithell,† Mike J. Goringe,† and Mike Bowker*

*Reading Catalysis Centre, Department of Chemistry, University of Reading, P.O. Box 224, Whiteknights, Reading RG6 6AD, United Kingdom; and †Department of Materials, University of Oxford, Parks Road, Oxford OX1 3PH, United Kingdom

Received October 12, 1995; revised May 1, 1996; accepted May 31, 1996

Two mixed Fe–Sb oxide catalysts were investigated for the selective oxidation of propene to acrolein and the ammoxidation of propene in the presence of ammonia to acrylonitrile. The techniques used were chiefly X-ray photoelectron spectroscopy (XPS), temperature deprogrammed desorption (TPD), X-ray diffraction, and transmission electron microscopy. After propene dosing TPD experiments were carried out in the absence of gas phase oxygen utilising lattice oxygen for oxidation. The samples contained a 1 : 1 and 2 : 1 atomic ratio of Sb : Fe (referred to as SbFe and Sb2Fe, respectively). XPS data indicate that the surface has an antimony oxide enriched selvedge which favours the selective ammoxidation of propene. The Sb enriched surface of SbFe was found to be highly reducible in low pressures of ammonia, yielding a metallic antimony overlayer. Subsequent thermal desorption of this metal coating revealed a surface with an increased iron (III) oxide content which was not so easily reduced and found to be of a lower selectivity to partial ammoxidation products. The Sb2Fe sample was more stable towards reduction.

1. INTRODUCTION

The catalytic, selective partial oxidation of propene to acrolein and in the presence of ammonia to acrylonitrile (ammoxidation) are commercially very important reactions (1, 2). A number of catalysts are selective for these reactions, including mixed iron–antimony oxide, which with additives (mainly bulk modifiers) such as W and Te forms a commercial catalyst for ammoxidation (3). Increased selectivity to acrolein has been obtained in microreactor studies using Sb-rich catalysts (4–8). A variety of proposals have been made previously for the enhanced selectivity of Sb-rich Fe–Sb oxides in the selective oxidation of olefins, including: (a) the formation of a surface compound of stoichiometry $FeSb_2O_6$ (4–6), (b) phase co-operation between the $FeSbO_4$ and Sb_2O_4 phases involving the migration of either oxide ions or an allyl intermediate between the two phases (7), (c) the formation of highly selective islands of Sb_2O_4 on top of the $FeSbO_4$ particles (8), (d) inhibition of the formation of free Fe_2O_3 and suppression of total oxidation (9).

In order to obtain a better understanding of the operation of these catalysts a number of previous studies have been carried out into the catalytic properties of a range of mixed Fe–Sb oxide catalysts together with the individual oxides of Fe and Sb. Previous studies have mostly employed continuous flow microreactor techniques as the principal method of measuring the catalytic activity of catalysts both in the presence and in the absence of gas phase oxygen. Complementary pre- and postreactor X-ray diffraction (XRD) measurements were often also taken to identify bulk changes in structure and composition brought about by the catalytic process. In contrast this study consists chiefly of X-ray photoelectron spectroscopy (XPS) and temperature programmed desorption (TPD) measurements carried out in high vaccuum conditions to investigate both surface composition and catalytic activity under well defined conditions. These investigations have been combined with transmission electron microscopy (TEM) for detailed structural identification of the catalyst materials.

The catalytic oxidation of propene and the ammoxidation of propene (from propene and NH_3), both in the absence of gas phase O_2, were investigated. We have additionally investigated compositional changes in the catalyst with a range of reduction/oxidation treatments using chiefly XPS and have determined their effect on catalytic activity using TPD.

Two mixed oxide materials were used in this study: the first was stoichiometric $FeSbO_4$ (referred to as SbFe) and the second contained Fe and Sb in the atomic ratio 1 : 2 (Sb2Fe). Subsequent publications will deal with the individual oxides of Fe and Sb. This publication expands on an earlier publication which dealt exclusively with propene oxidation on SbFe (10) including additional data relating to Sb2Fe and to ammoxidation.

2. EXPERIMENTAL

The SbFe oxide catalyst was prepared by a slurry impregnation method (4). $Fe(NO_3)_3 \cdot 9H_2O$ was heated to 333 K in a Pyrex beaker on a hot plate/magnetic stirrer, at which

0021-9517/96 $18.00

temperature a solution of iron nitrate in its own water of crystallisation was formed; Sb_2O_3 was added (brown fumes were liberated at this stage), the temperature was raised to 350 K and the solution pH was adjusted to 3.0 using aqueous ammonia. The brown solid was recovered by filtration and dried (400 K, 16 h); it was then calcined in air at atmospheric pressure at 1173 K for 7 h to give interdiffusion of the cations. The 2 : 1 Sb : Fe oxide catalyst was prepared in a similar fashion although the quantities of $Fe(NO_3)_3 \cdot 9H_2O$ and Sb_2O_3 were adjusted to give the correct Sb : Fe ratio. The antimony oxides (III, IV, and V) were used as supplied by Aldrich.

XPS measurements were carried out using a VSW system with 100-mm radius hemispherical analyser and Al$K\alpha$ photons. The sample was pressed on a stainless steel mesh with a chromel–alumel thermocouple attached, and this was mounted on an x–y–z rotational manipulator. The spectra were referenced to the Au($4f_{7/2}$) line at 83.9 eV and to the adventitious C(1s) line at 284.8 eV. TPD was carried out by radiative heating of the sample from a tungsten filament heater situated close to the rear of the sample at a ramp rate of $\sim$3 K s^{-1}. Desorption profiles were measured using a VG quadrupole mass spectrometer. Dosing was carried out with the sample at $\sim$300 K, with 10-min exposures at pressures of 1×10^{-2} or 1×10^{-4} mbar for propene and ammonia, respectively. The masses of the major species monitored was as follows: acrolein, 56; acrylonitrile, 53; propene, 41; CO_2, 44; H_2O, 18. The weight of the catalyst used was typically 0.2 g. The XPS background subtraction method used was a Proctor/Hercules modified Shirley integration (11). Determination of the iron : antimony surface atomic ratio was calculated from the relative peak areas of the Sb(3d) and Fe(2p) transitions after subtraction of the O(1s) content from the Sb($3d_{5/2}$) peak (assuming a 3 : 2 ratio of $3d_{5/2} : 3d_{3/2}$). The relative cross-sectional sensitivities of Sb(3d) to Fe(2p) were taken as 4.47 : 2.67, respectively (12). The difference between the escape depths of iron and antimony electrons was assumed to be negligible. Prior to surface area determination samples were heated in an atmosphere of nitrogen to 423 K. The surface area measurements were calculated using a BET procedure and Micromeritics Gemini equipment. The XRD powder diffraction data were recorded using an Inel Spectrolab CPS 120 using Cu$K\alpha$ radiation and operated at 40 kV and 40 mA.

TEM characterisations were carried out using various instruments operating at 200 and 400 kV, as specified in the figure captions. Specimens for TEM examination were prepared by ultrasonically dispersing small amounts of the catalyst in methanol and allowing drops of the resulting suspensions to dry on standard amorphous carbon films supported on gold or copper specimen grids.

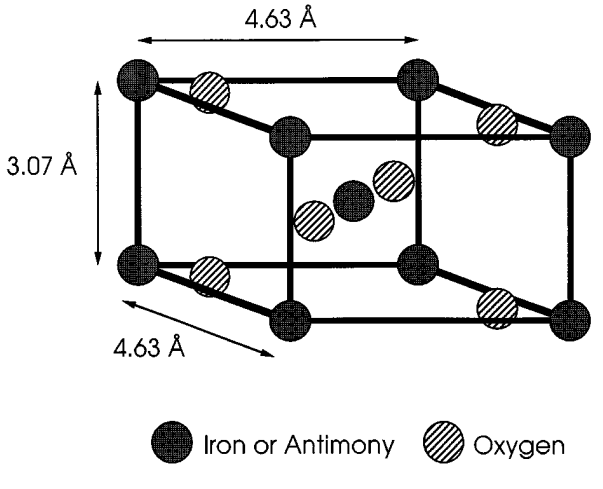

FIG. 1. Schematic of the ideal rutile type structure of $FeSbO_4$.

3. RESULTS AND DISCUSSION

3.1. Structure and Composition of Catalyst Samples

Initial characterisation of the samples came from TEM and XRD analysis. These techniques indicated that the bulk of the SbFe material was dominated by a single phase of $FeSbO_4$ with a statistical rutile structure (13), a schematic of which is shown in Fig. 1. This is in general agreement with previous work on $FeSbO_4$ (8) though the precise ordering of the cations is the subject of some debate (14). The structure represented in Fig. 1 is therefore an idealised one. Figure 2a shows a high resolution TEM image of a single catalyst particle of $FeSbO_4$ from the SbFe material. The bulk structure shows a single phase with lattice parameters consistent with $FeSbO_4$. The XRD diffractogram of the fresh catalyst (Fig. 3a) contained three major peaks at 2θ values of 27.1°, 35.6°, and 53.2°, which are characteristic of the rutile structure of $FeSbO_4$. The uncalcined, dried SbFe was found to be completely amorphous in XRD, indicating that the high temperature calcination is required to produce interdiffusion of the ions and to form an ordered structure. Characterisation of the calcined Sb2Fe material by TEM showed that it contained at least two distinct phases ($FeSbO_4$ and α-Sb_2O_4) with the former apparently having a bimodal distribution of particle size, as illustrated in Figs. 2b–2d. The $FeSbO_4$ phase was identified from its electron diffraction patterns, which are those of a rutile structure with the $FeSbO_4$ lattice parameters. There was no detectable difference in structure or composition between the large and the small $FeSbO_4$ particles (Figs. 2b and 2c, respectively) as far as imaging or diffraction behaviour is concerned. The very large particles (e.g., Fig. 2d) were identified as single crystals of antimony oxides from their diffraction patterns. Most of these could be indexed as coming from α-Sb_2O_4, although a few were difficult to index or could be attributed to other SbO_x phases. These identifications were substantiated by energy dispersive X-ray (EDX) spectra. The large

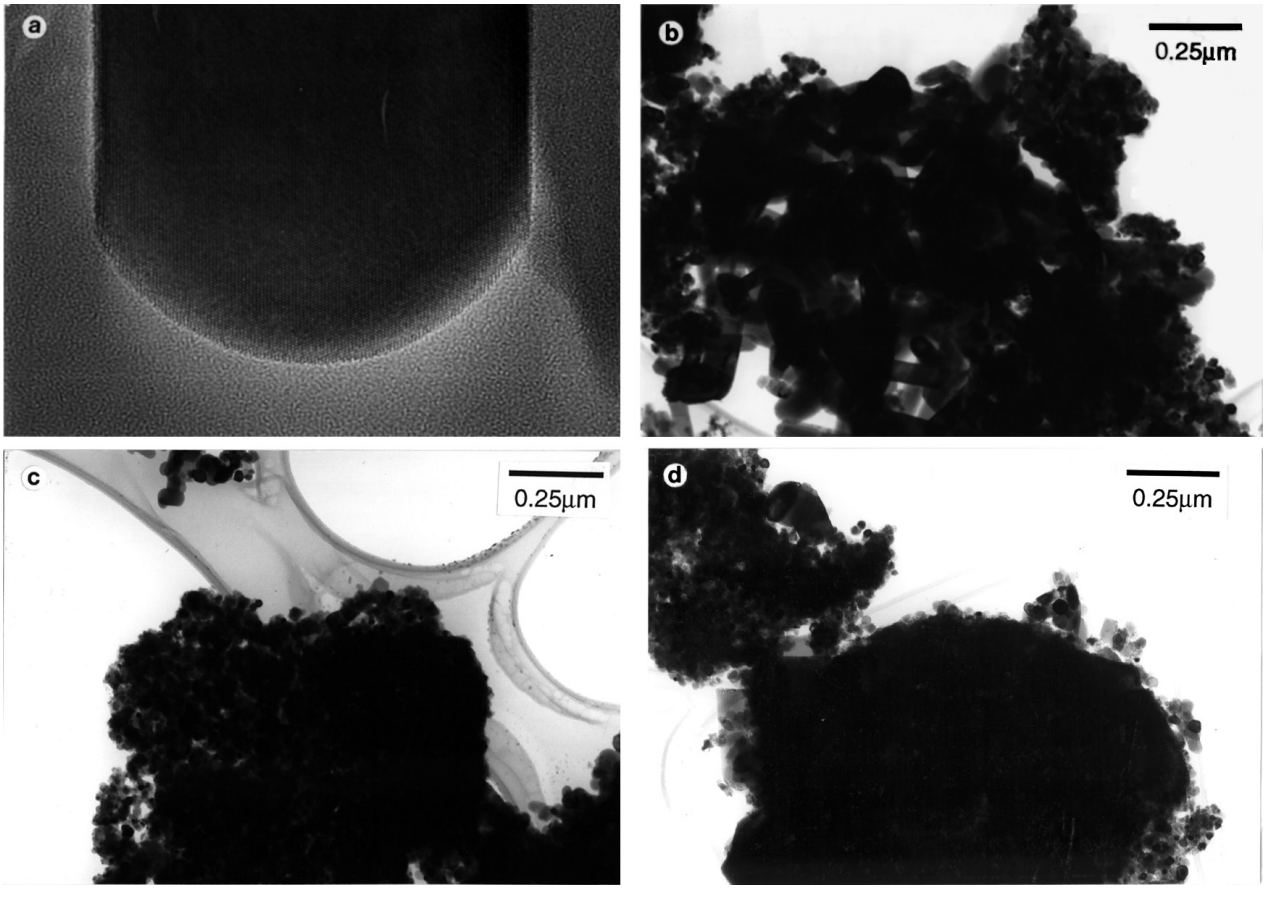

FIG. 2. (a) High resolution TEM image of an $FeSbO_4$ particle from the SbFe catalyst showing a single, well ordered phase obtained using a JEOL 4000EX instrument operating at 400 kV. A ⟨111⟩ zone axis is parallel to the electron beam and the 0.327 nm {110} lattice fringes run vertically. Magnification approximately 3×10^6. (b) Conventional TEM bright field image of an agglomeration of (mostly) large, faceted $FeSbO_4$ particles from the Sb2Fe catalyst, very similar to those which make up the SbFe catalyst. This image and those comprising (c) and (d) were obtained using a JEOL 200CX TEM operating at 200 kV. (c) Bright field image of small $FeSbO_4$ particles in the Sb2Fe catalyst. (d) Bright field image of a large antimony oxide particle from the Sb2Fe catalyst, decorated with smaller $FeSbO_4$ particles.

antimony oxide particles showed essentially no Fe counts (those which were collected from these particles could easily be attributed to neighbouring $FeSbO_4$ particles). There was, however, a systematic difference in the EDX spectra for the $FeSbO_4$, as a function of particle size, in that the relative proportion of Sb to Fe counts increased as the particle size decreased. It is not possible to be certain where the extra Sb is located: it could be as "free" antimony oxide incorporated as nonstoichiometry into the bulk of the $FeSbO_4$, or present as a surface layer. Both of these would be difficult to detect by TEM imaging/diffraction techniques. However, the observed smooth increase in Sb counts with decreasing particle size suggests that the last explanation may be the correct one and this would indeed be consistent with the Sb enriched surface layer observed with XPS for $FeSbO_4$ in the SbFe material. The XRD of Sb2Fe (Fig. 3a) contained peaks attributable to both $FeSbO_4$ and Sb_2O_4. The XRD of Sb_2O_4, is also shown in Fig. 3a for comparison. This XRD pattern is for a commercial Sb_2O_4 sample which contained both α and β phases of the oxide; these phases are identified in Fig. 3b. The additional features observed in the Sb2Fe diffractogram compared with SbFe do not therefore coincide with all the peaks in the Sb_2O_4 diffractogram but only the component of this pattern attributable to its α-Sb_2O_4 component. Closer inspection of the XRD data showed that the peaks attributable to $FeSbO_4$ are broader in the Sb2Fe sample than in the SbFe; this can be attributed to the presence of smaller $FeSbO_4$ particles, identified in Sb2Fe by TEM. Figure 3c shows a comparison of one of the major diffraction peaks of $FeSbO_4$ from the SbFe and the Sb2Fe material, clearly showing that the latter is broader (the FWHM of the peak at 2θ value 35.6° was 0.28° for SbFe and 0.47° for Sb2Fe).

The BET surface area of the SbFe catalyst sample, and its precursor compounds, was measured at various points in the preparation. The results are shown in Table 1. The precursor Sb_2O_3 has a relatively low surface area although the uncalcined SbFe produces a sample with a much higher

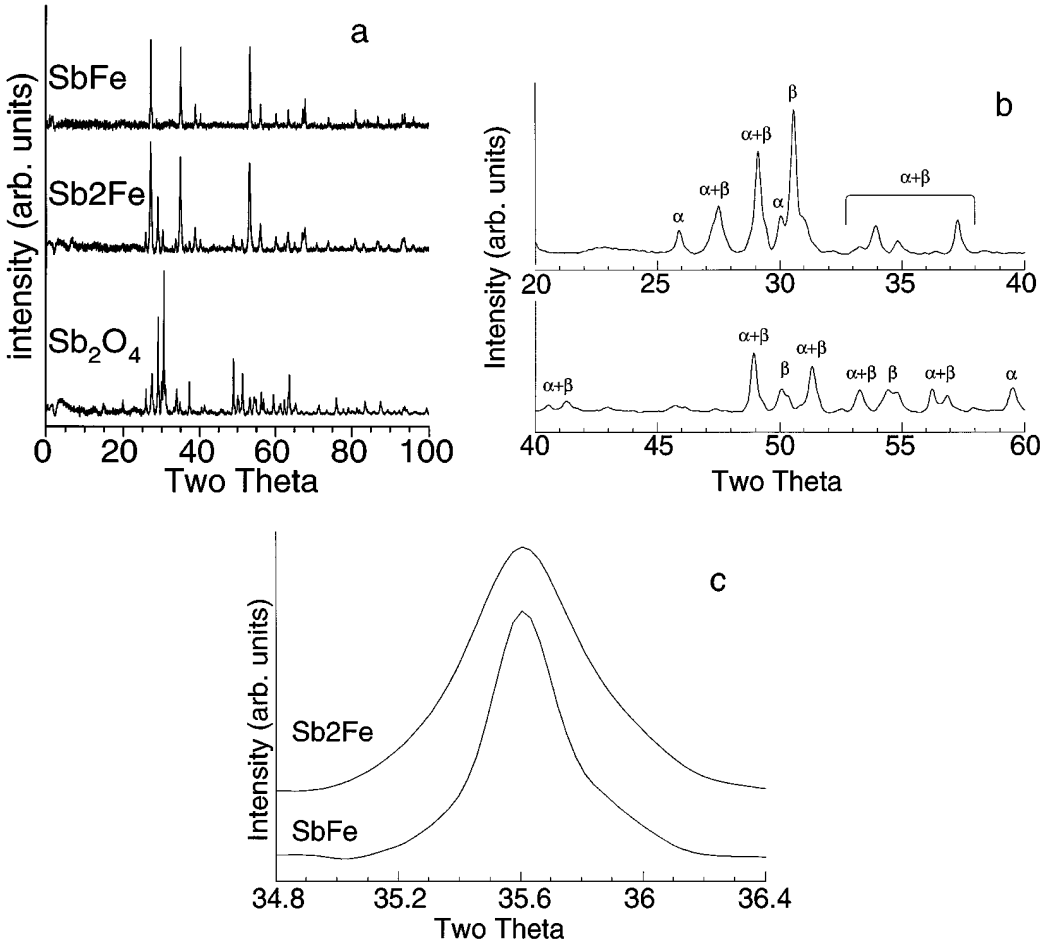

FIG. 3. XRD diffractograms: (a) untreated, calcined SbFe, Sb2Fe, Sb_2O_4. (b) Sb_2O_4 with α and β phases labeled. (c) Comparison of peak widths for $FeSbO_4$ in the SbFe and the Sb2Fe material.

surface area. The final calcination stage of the preparation led to a reduction in the surface area by an order of magnitude. Granulation, by pressing the sample into pellets then crushing, had little effect on the surface area. The higher surface area of the Sb2Fe compared with that of SbFe is consistent with the smaller particle size in Sb2Fe observed with XRD and TEM.

X-ray photoelectron spectra of the fresh SbFe and Sb2Fe samples, taken after heating in vaccum at ~800 K, are shown in Fig. 4. Figure 4a shows a survey scan of the SbFe catalyst. With the exception of a small C(1s) peak all significant peaks could be assigned to photoemission and Auger transitions of Fe, Sb, and oxygen as indicated. The Fe($2p_{3/2}$) peak (Fig. 4b) at 711.5 eV binding energy (BE) indicated that iron was predominantly in the 3+ oxidation state for both SbFe and Sb2Fe (15). Significant Fe^{2+} at the surface can be excluded as it would be expected to produce a noticeable shoulder at lower binding energy on the Fe($2p_{3/2}$) peak. Identification of the oxidation state of the Sb is more problematic as the separation in the BE of Sb^{3+} and Sb^{5+} is only ~0.3 eV (16). An added complication is that the Sb($3d_{5/2}$) peak almost exactly overlaps with that of O(1s) at ~531 eV BE (Fig. 4c). Some debate exists in the literature as to the oxidation state of the Sb in the surface layer with both an exclusively 5+ (17) and a mixed 5+/3+ surface being suggested (4, 6). Our XPS data cannot conclusively distinguish between the two proposals. The Sb($3d_{3/2}$) transition is, however, well resolved from other peaks and can be used for both quantitative analysis of the Sb composition and also, to some degree, for the identification of the chemical state

TABLE 1

BET Surface Areas of Samples at Various Stages of the Preparation Procedure

Sample	BET surface area (m^2/g)
Sb_2O_3	2.3
$FeSbO_4$, dried at 373 K	42.8
$FeSbO_4$, calcined at 1173 K	5.9
Sb2Fe, calcined at 1173 K	8.8

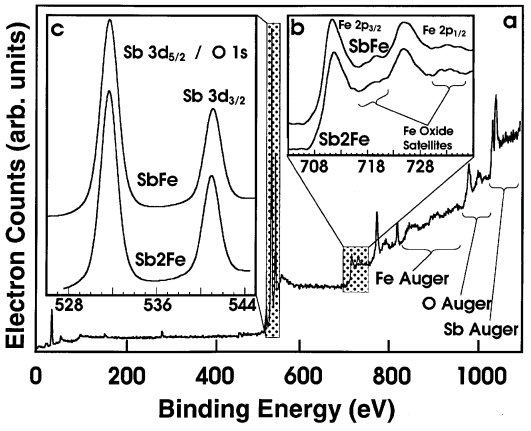

FIG. 4. X-ray photoelectron spectra of SbFe and Sb2Fe after heating to 800 K in vacuum: (a) wide scan of SbFe showing principal transitions, (b) Fe(2p) region of SbFe and Sb2Fe, (c) Sb(3d)/O(1s) region of SbFe and Sb2Fe.

of the Sb, in distinguishing for example, between Sb metal, Sb^{3+}, and Sb^{5+}.

Quantitative analysis of the Sb(3d) and Fe(2p) photoemission peaks was carried out in order to determine the surface composition in the SbFe catalyst. Instead of the 1 : 1 ratio expected from the bulk stoichiometry, comparison of the relative areas of the Fe(2p) and Sb(3d) peaks indicated a selvedge with an Fe : Sb ratio of ~1 : 2. The presence of an Sb-enriched surface agrees with the work of several previous studies (4, 8, 17, 18). Aso *et al.* (4) proposed a surface compound of composition $FeSb_2O_6$ for Sb : Fe $\geq$ 1 in order to account for this Sb enrichment. This conclusion was supported by XPS spectra indicating Fe^{2+} species at the surface. However, in the present work no evidence was found for Fe species other than 3+ at the surface of either mixed oxide sample. Another explanation for the Sb enrichment has been offered by Teller *et al.* (8), who propose Sb_2O_4 crystallites at the surface of the $FeSbO_4$ particles, although our TEM results show no evidence for this. It is also possible that the termination of the $FeSbO_4$ lattice is such that Sb cations dominate in the surface region (10) and this explanation cannot be excluded by our TEM images in that we have no explicit evidence of the presence or absence of such an enriched layer.

3.2. Reduction of Catalyst Surface with NH_3

In the industrial ammoxidation reaction the catalyst is exposed to a gas phase mixture of propene, NH_3, and oxygen. It is therefore interesting to investigate the effect of these gases individually on the catalyst. This section deals with changes in the surface composition of mixed Sb–Fe oxides when heated in NH_3 as this treatment produces a number of interesting results of relevance to understanding the reactivity of the catalysts investigated. The effect on the catalyst composition and reactivity after oxygen and propene treatments is dealt with in the next section together with information on changes in the reactivity of SbFe and SbFe after NH_3 treatments. It should be noted that although TPD experiments were carried out under anoxic (absence of oxygen) conditions, the catalyst was tested in a microreactor with gas phase oxygen and results were found to be in agreement with published literature.

After only a mild treatment in ammonia (520 K, 2×10^{-4} mbar for 20 min) the Sb in the surface layer of SbFe could be reduced to the metal, as shown in the XPS of the Sb(3d) region in Fig. 5a. A second Sb($3d_{3/2,\,5/2}$) doublet peak was observed shifted by 2.0 eV to lower binding energy, an effect which could only be produced by formation of Sb^0 metal. This was confirmed by TPD (Fig. 5b) which showed Sb desorption with a peak maximum at 690 K. Following ammonia reduction there were no signs of significant Fe^{2+} formation. Reduction to Fe^{2+} can, however, occur under more severe reducing conditions: for example, reduction of an SbFe catalyst sample at ~800 K in 10 Torr H_2 led to the formation of Fe_3O_4 (13). The effect of annealing the NH_3 reduced sample to gradually higher temperature was also monitored using XPS. Figure 5 shows spectra taken (with the sample at 300 K) after annealing the reduced sample to gradually higher temperature. The gradual loss of the Sb metal peak is clearly seen from ~500 K. Following Sb desorption the XPS spectrum differed from that of the fresh sample with an Sb : Fe atomic ratio of 1 : 2.6; that is, Fe was much more dominant in the spectrum. This can be clearly seen from a comparison of the relative intensities of the Sb(3d) and Fe(2p) peaks in the XPS spectra of untreated

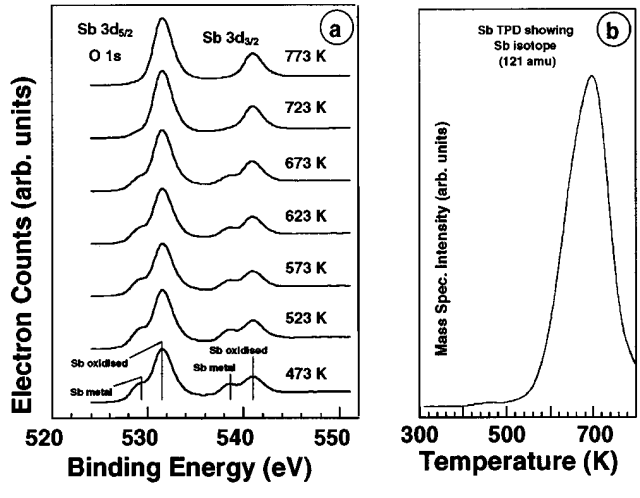

FIG. 5. (a) X-ray photoelectron spectra of Sb(3d) region in SbFe after heating the sample to 500 K in 2×10^{-4} Torr of NH_3 for ~30 min, showing the effect of annealing to gradually higher temperature. All spectra taken after sample was heated to the temperature indicated for 2 min and then allowed to cool below 350 K. The annealing temperature is shown alongside each spectrum. (b) TPD profile showing Sb metal desorption from NH_3 reduced SbFe.

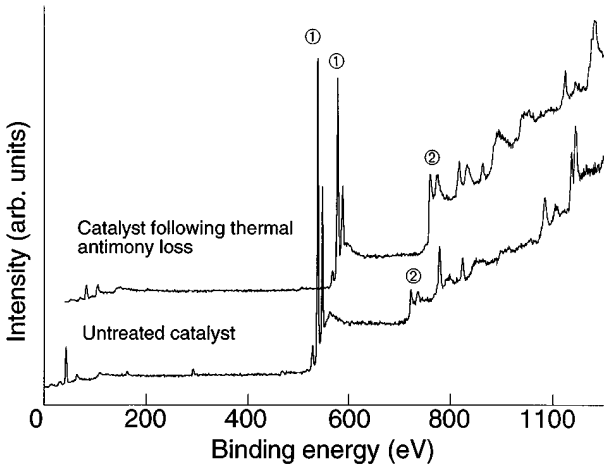

FIG. 6. X-ray photoelectron spectra of the SbFe material showing compositional changes on desorption of antimony metal following NH_3 reduction. Sb(3d) and Fe(2p) peaks are labeled 1 and 2, respectively. The top spectrum is offset for clarity.

and NH_3 reduced and annealed surfaces shown in Fig. 6. Prolonged annealing at 800 K did not alter the antimony to iron atomic ratio, that is, the iron enriched surface phase was found to be stable. Rather than being desorbed the matallic Sb layer produced by reduction in NH_3 could also be completely reoxidised by heating at 500 K in O_2. This procedure resulted in a surface with similar composition to the starting material.

A similar NH_3 reduction treatment of the 2 : 1 Sb : Fe material did not lead to the observation of Sb metal at the surface even though 50% of the Sb in this catalyst is present in the $FeSbO_4$ component, which in the single phase SbFe catalyst has been shown to be reducible to the metal under these conditions. Additional single oxide work was carried out on Sb_2O_4, a component of the Sb2Fe catalyst, which showed that under these conditions Sb_2O_4 did not reduce to the metal according to XPS analysis following reduction. It is therefore clear that the $FeSbO_4$ component in the Sb2Fe catalyst is stabilised by the presence of the Sb_2O_4. In this respect it is interesting to note that a 1 : 1 by weight mixture of $FeSbO_4$ and Sb_2O_4 could be reduced to produce Sb metal at the surface with a treatment of heating in 2×10^{-4} mbar NH_3 at 520 K for 20 min. Figure 7 shows the Sb(3d)/O(1s) region XPS spectra for the physical mixture and the Sb2Fe after the NH_3 reduction procedure. An Sb metal peak (indicated on the figure) is clearly distinguishable as a low energy shoulder to the Sb oxide(3d)/O(1s) peak in the physical mix sample. The intensity of this Sb metal peak is lower than in the NH_3 reduced SbFe catalyst due at least in part to the lower amount of reducible Sb in the physical mix catalyst; only 40% of the Sb is in the $FeSbO_4$ phase, the remainder being contained in the unreduced Sb_2O_4 phase. No shoulder was observed with the Sb2Fe catalyst even though the reducible Sb content is a little higher (50%). These results suggest that formation of an Sb metal coating in Sb2Fe is prevented by a more intimate association of the two compounds (SbFe and Sb_2O_4) in Sb2Fe than in the physical mixture.

There have been several possible explanations for the role of excess antimony oxide proposed in the literature to account for the difference in behaviour between SbFe and Sb2Fe. These include: (1) differences in the structure/composition of the $FeSbO_4$ phase when formed in the presence of excess Sb, (2) crystallites of Sb_2O_4 on the surface of $FeSbO_4$ in the presence of excess antimony oxide, (3) production of a surface phase in the $FeSbO_4$ particles of Sb2Fe not found in FeSb, (4) phase interface effects in Sb2Fe. Our TEM results suggest that 1 and 2 are unlikely though they provide no conclusive evidence for 3 or 4. A proposed mechanism for a phase interface effect could be the diffusion of oxygen ions from the Sb_2O_4 to the $FeSbO_4$ particles. Such a diffusion could occur through the boundaries where the two phases are in contact and such contact points would be more abundant in the Sb2Fe material where the final material has been subjected to a high temperature calcination than in the simple physical mixture of SbFe and Sb_2O_4.

Phase co-operation in these types of catalyst materials is a well known phenomenon (19). For example, phase cooperation has been previously associated with the higher selectivity of Sb2Fe compared with that of SbFe (7). One of the most common mechanisms proposed is that of oxygen spillover which is generally considered to occur across the surface and involves the dissociation of gas phase molecular oxygen present in many microreactor studies of propene partial oxidation (20). It has been suggested by Weng *et al.* (21) that the beneficial effects of Sb_2O_4 in mixed phase

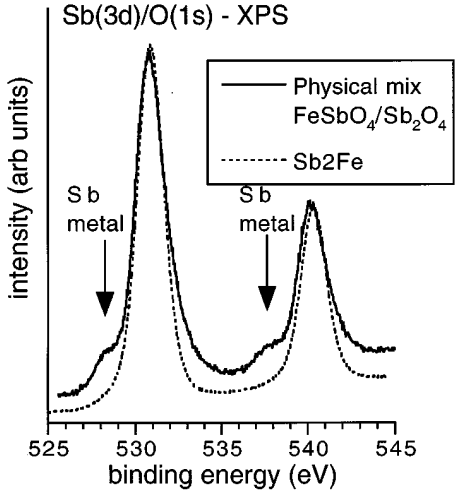

FIG. 7. X-ray photoelectron spectra of the Sb(3d)/O(1s) region in two NH_3 reduced samples: Sb2Fe and a 1 : 1 physical mixture by weight of $FeSbO_4$ and Sb_2O_4.

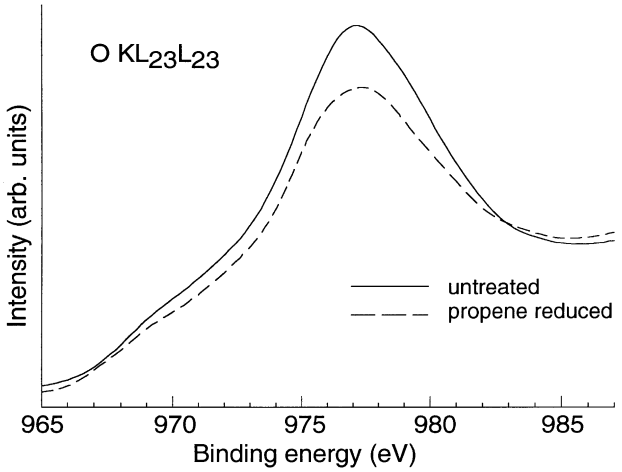

FIG. 8. X-ray excited oxygen KLL Auger spectra for a fresh and propene reduced SbFe catalyst. The spectra are normalised to the same $Sb(3d_{3/2})$ peak intensity.

catalysts of this kind can be explained by its ability to produce spillover oxygen which reacts with the surface of another oxide to improve its properties, e.g. to maintain its surface oxide ions in a particular oxidation state. This mechanism is similar to that suggested here though the "spillover oxygen" cannot be from the gas phase and so must be supplied from the Sb_2O_4 lattice. Other authors have indeed suggested that oxygen transport through the lattice could be of significant importance in producing a stable surface phase and so maintaining a catalyst's ability to produce selective oxidation of hydrocarbons (22). As outlined below, there is a link between selectivity to partial oxidation and stability towards NH_3 reduction and so phase co-operation involving lattice oxygen can be suggested as the mechanism to account for this. Conclusive evidence for oxygen diffusion between the $FeSbO_4$ and Sb_2O_4 phases would be difficult to obtain although ^{18}O tracer studies of the type empolyed by other workers would no doubt be of value (22).

3.3. TPD Studies

The fresh samples were found to be extremely unselective, the propene initially being completely burned with no acrolein/acrylonitrile formation. After several adsorption/desorption cycles the selectivity of the catalyst to partial oxidation products was achieved. This phenomenon has been observed in microreactor studies by Fattore *et al.* (7) using Sb–Fe–O to oxidise propene in the absence of oxygen and also in TPD studies with SbFe oxides (18, 23). A somewhat reduced surface, which can be achieved by several

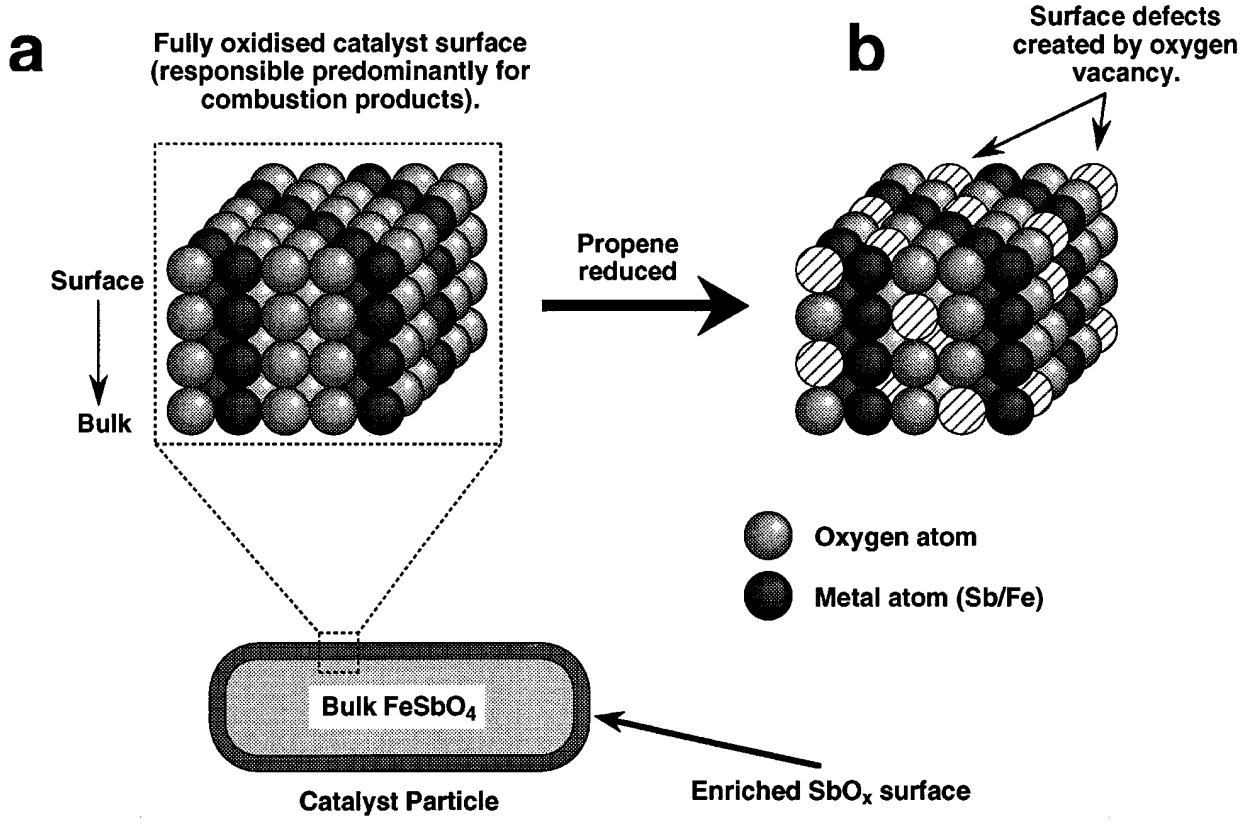

FIG. 9. Schematic showing the different oxygen species on the catalyst surface and their role in determining selectivity to partial oxidation products.

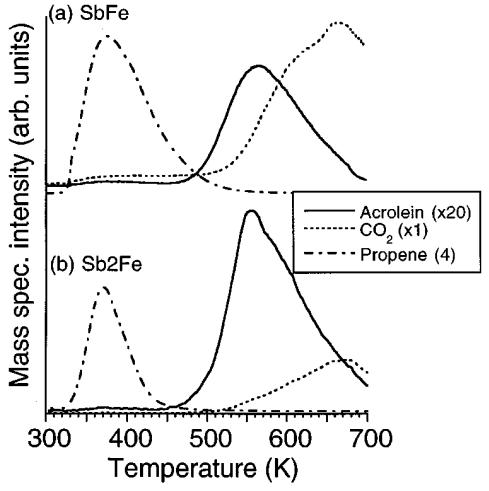

FIG. 10. TPD profile showing the most significant desorption products following a propene dose of 5×10^{-3} Torr for 10 min on (a) SbFe and (b) Sb2Fe. Intensities are not corrected for the relative sensitivity of the mass spectrometer to different species.

propene dose/TPD cycles, is therefore required for selective oxidation. This is supported by the data in Fig. 8, indicating that repeated propene dose/TPD cycles led to a small (10%) reduction in the measured oxygen content of the SbFe sample. Figure 8 shows the oxygen KLL X-ray excited Auger peaks for a SbFe catalyst sample after initial outgassing and then after several propene dose/TPD cycles. The small decrease in the measured oxygen signal can be attributed to a higher concentration of oxygen vacancies in the selvedge region than were present in the fresh catalyst. Initially there is a high concentration of oxygen atoms on the surface which favours complete oxidation. The formation of anion vacancies lowers the probability of finding the critical surface ensemble with the required number of oxygen ions for complete oxidation and so favours oxidative dehydration to the allylic intermediate which has a lower oxygen requirement. These oxygen vacancies therefore produce the increased selectivity to partial as opposed to complete oxidation (combustion) products of H_2O and CO_2. A schematic representation of this mechanism is shown in Fig. 9. Consistent with these results, Grasselli and Suresh (24) have proposed a model for the selective partial oxidation of propene which requires an oxygen vacancy adjacent to the Sb ion in order to facilitate formation of an allyl intermediate thought to be necessary for selective oxidation. It has been suggested by Landa-Cánovas *et al.* (25) that cation vacancies, not the formation of anion vacancies, are responsible for the increased selectivity in a related material, $SbVO_4$. However, this can be ruled out as no alteration of the antimony to iron atomic ratio was found in XPS to accompany this change in selectivity.

After the initial period of high combustion behaviour the surface composition and reactivity of the samples were essentially invariant with repeated propene–ammonia dose/TPD experiments. This indicates that the efficient diffusion of oxygen from the bulk to replenish surface oxygen lost in oxidation reactions occurs via a mechanism similar to that proposed by Mars and van Krevelen for bismuth molybdate catalysts (2). The catalyst could be returned to the unselective initial state by oxygen treatment in vacuum; selectivity was again achieved after several adsorption/desorption cycles. The consumption of lattice oxygen in the oxidation process would be expected to lead eventually to bulk reduction of the sample and loss of selectivity (7). However, the total amount of oxygen consumed over 20 or so dose/TPD cycles was not sufficient for this process to be observed.

(a) Partial oxidation of propene. After the initial induction period the SbFe catalyst was a reasonably selective oxidation catalyst yielding significant amounts of acrolein in an experiment for which only propene was dosed onto the surface, the relative integrated peak areas of acrolein and CO_2 being approximately 1:2 (allowing for the different sensitivity of the mass spectrometer to the two gases). A typical temperature programmed desorption profile showing the most significant desorption products is shown in Fig. 10a. Figure 10b shows the equivalent desorption profiles for the Sb2Fe sample which can be seen to show increased selectivity to acrolein, the relative peak areas of acrolein to CO_2 being 1:8. The increased selectivity to acrolein of Sb-rich catalysts has been reported by several authors (4–8) and has been attributed to phase co-operation between $FeSbO_4$ and Sb_2O_4. This phase co-operation could take the form of oxygen ion migration from Sb_2O_4 to $FeSbO_4$, a mechanism invoked above to

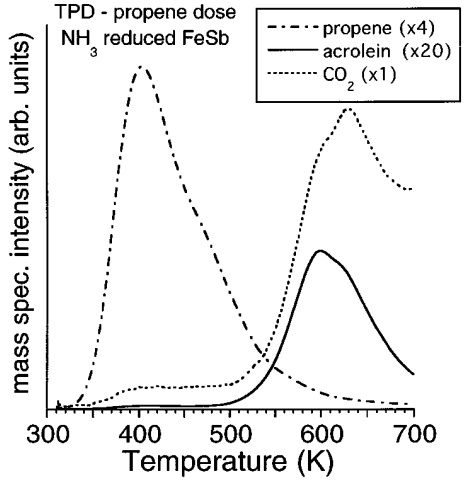

FIG. 11. TPD profile showing the most significant desorption products from a SbFe sample following a propene dose of 5×10^{-3} Torr for 10 min after the sample was pretreated by NH_3 reduction and Sb^0 desorption. Intensities are not corrected for the relative sensitivity of the mass spectrometer to different species.

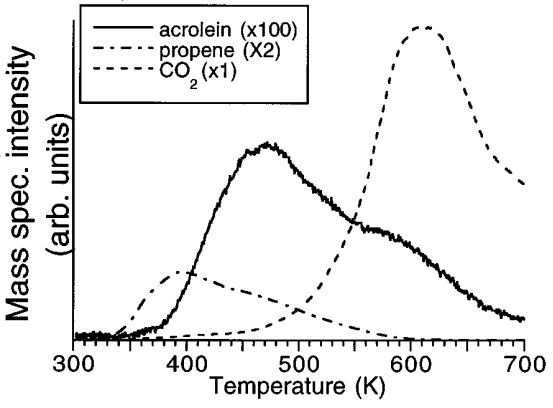

FIG. 12. TPD profile following propene dose (10 min 2×10^{-6} mbar) on iron oxide.

describe the greater stability of Sb2Fe towards NH_3 reduction. A single oxide sample of Sb_2O_4 was tested in similar conditions to Sb2Fe and showed no measurable activity during TPD studies. This is in agreement with microreactor studies of Sb_2O_4 which have shown a measurable but very low activity for the selective oxidation of propene (26). This demonstrates that the Sb_2O_4 component of the Sb2Fe material leads only to an increase in selectivity due to its presence in conjunction with the $FeSbO_4$ component.

In both sets of profiles (Figs. 10a and 10b) propene was desorbed at ~400 K. Complete oxidation products CO, CO_2, and H_2O are desorbed in significant quantities at higher temperature. Acrolein desorption peaks at ~570 K. It can be seen that the instantaneous selectivity toward acrolein was greater on the low temperature side of the desorption peak and was reduced at the expense of complete oxidation products at higher temperature.

After ammonia reduction of SbFe and desorption of the "metallic" antimony formed, subsequent propene dosing produces an altered desorption profile, showing decreased total acrolein yield and selectivity and much reduced acrolein selectivity at any given temperature (Fig. 11). The surface layer left after reduction and Sb desorption was enriched in Fe oxide which has been shown to be low in selectivity to acrolein formation (27), favouring formation of complete oxidation products. This point is further demonstrated by our work on propene TPD studies from iron oxide illustrated in Fig. 12. This figure shows the considerably lower selectivity of iron oxide to the partial oxidation of propene when compared with SbFe. The selectivity of $FeSbO_4$ to selective oxidation products is therefore demonstrated to be dependent on the Sb-enriched surface layer.

(b) Ammoxidation of propene. Figure 13 shows a typical thermal desorption profile taken after sequential adsorption of propene and NH_3 on the SbFe and Sb2Fe samples. Again both unreacted (NH_3, propene), completely oxidised (CO_2, H_2O, NO), and partial oxidation products (acrylonitrile, acrolein) were observed. The acrylonitrile desorption peak maximum occurred at ~520 K and then fell rapidly as CO_2 production rose. Other nitrogenous species were desorbed mainly in the form of NO and N_2. These species produced broad relatively featureless desorption traces increasing greatly in intensity at temperatures >550 K. Similar high temperature desorption of nitrogenous species were also observed when NH_3 only was adsorbed, confirming that these products result from the oxidation of the NH_3.

In experiments where the propene : ammonia dose ratio was sufficiently high, both acrylonitrile and acrolein were desorbed coincidentally, the yield of acrylonitrile relative to acrolein increasing with the NH_3 : propene dose ratio. This can be seen in Fig. 13b for the Sb2Fe sample. The coincident desorption of acrolein and acrylonitrile suggests that

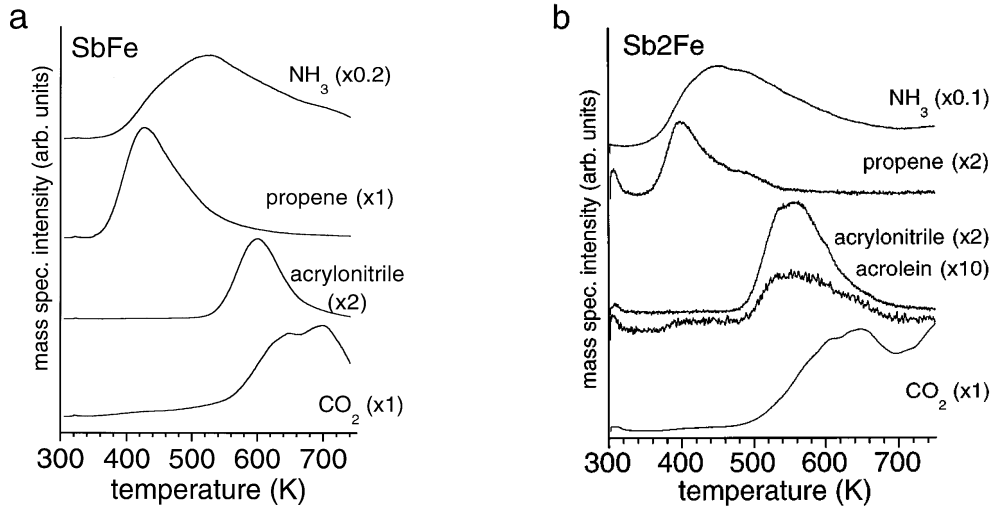

FIG. 13. Thermal desorption profile taken after sequential adsorption of propene and NH_3 on (a) SbFe and (b) Sb2Fe. Intensities are not corrected for the relative sensitivity of the mass spectrometer to different species.

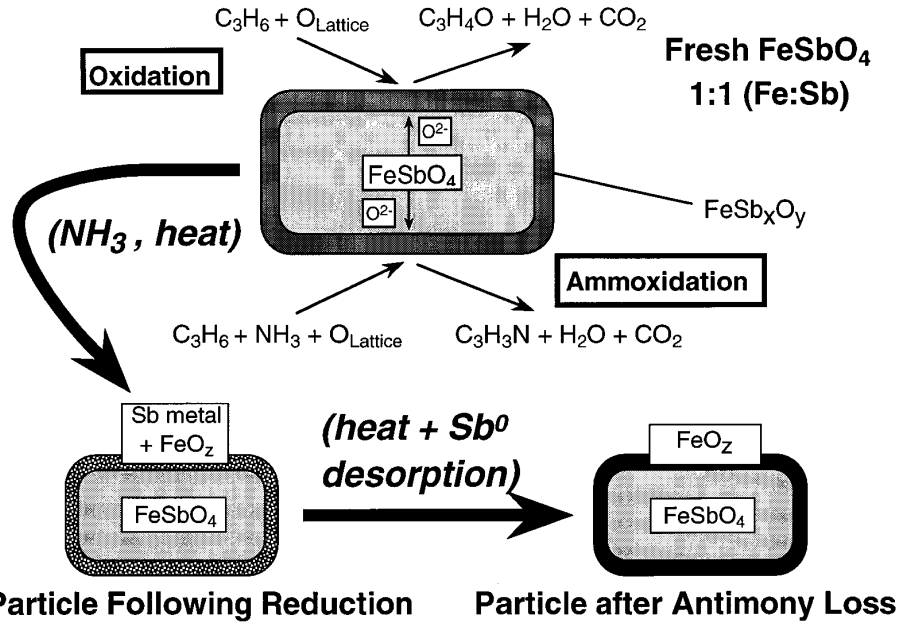

FIG. 14. Schematic summarising the changes in surface composition and reactivity of the SbFe catalyst sample which can be produced by reduction in NH_3.

the oxidation and ammoxidation reactions have a common rate determining step. This is consistent with a single pass flow reactor study of the selective oxidation of propene over iron–antimony oxide (atomic ratio Sb/Fe = 4), identifying the rate determining step as the abstraction of an allyl hydrogen from propene, a common step for the two reactions (28).

4. CONCLUSIONS

1. Desorption of acrylonitrile and acrolein were observed in TPD using mixed Fe–Sb oxide powder samples after exposure respectively to a propene and ammonia mix or propene alone.

2. SbFe was readily reduced by heating at 500 K in NH_3 to produce Sb metal at the surface. This metal layer could be desorbed on heating, leaving an Fe-enriched surface which had a lower selectivity toward acrolein/acrylonitrile formation than the original surface, which by contrast was Sb-enriched in the selvedge region. The Sb-enriched surface of $FeSbO_4$ therefore plays a crucial role in the selectivity of this material. It is interesting to note that recent work by Moro-oka *et al*. indicates that the reactivity of bismuth–molybdate catalysts towards acrolein synthesis can similarly be linked to a surface region of different composition to the bulk (22). The relationship between surface composition and reactivity for SbFe is summarised schematically in Fig. 14. Sb2Fe was not reduced to the metal under the same conditions and its selectivity to acrolein production was therefore not affected by the reduction treatment.

3. SbFe and Sb2Fe require slight reduction of the surface to avoid combustion of the propene. This can be produced by several propene dose/TPD cycles.

4. The enhanced stability of Sb2Fe to reduction with NH_3 could be linked to its greater selectivity towards acrolein production. This can be attributed to a migration of lattice oxygen from the Sb_2O_4 phase to the $FeSbO_4$ phase.

ACKNOWLEDGMENTS

The authors are pleased to acknowledge financial support from the University of Reading, the EPSRC, and BASF plc. E.G.B. is grateful to the EPSRC (Grant GR/H 34166) for financial support.

REFERENCES

1. Kung, H. H., *in* "Studies in Surface Science and Catalysis," Vol. 45, p. 169. Elsevier, Amsterdam, 1991.
2. Moro-oka, Y., Ueda, W., and He, D.-H., *in* "Dynamic Processes on Solid Surfaces" (Tamaru, K., Ed.), p. 283. Plenum, New York, 1994.
3. Yoshino, T., Saito, S., Sasaki, Y., and Nakamura, Y., Japanese patent 3 657 155 (1972), 3 686 138 (1972).
4. Aso, I., Furukawa, S., Yamazoe, V., and Seiyama, T., *J. Catal.* **64**, 29 (1980).
5. Sala, F., and Trifirò, F., *J. Catal.* **41**, 1 (1976).
6. Carbucicchio, M., Centi, G., and Trifirò, F., *J. Catal.* **91**, 85 (1985).
7. Fattore, V., Fuhrman, Z. A., Manara, G., and Notari, B., *J. Catal.* **37**, 223 (1975).
8. Teller, R. G., Brazdil, J. F., and Grasselli, R. K., *J. Chem. Soc. Faraday Trans. 1* **81**, 1693 (1985).
9. Shchukim, V. P., Boreskov, G. K., Ven'yaminov, S. A., and Tarasova, D. V., *Kinet. Katal.* **11**, 153 (1970).
10. Allen, M. D., and Bowker, M., *Catal. Lett.* **33**, 269 (1995).
11. Proctor, A., and Hercules, D. M., *Appl. Spectrocs.* **38**, 505 (1984).

12. Moulder, J. F., Stickle, W. F., Sobol, P. E., and Bomben, K. D., "Handbook of X-ray Photoelectron Spectroscopy." Perkin-Elmer, 1992.
13. Bithell, E. G., Doole, R. C., Goringe, M. J., Allen, M. D., and Bowker, M., *Phys. Status Solidi* **146**(a), 461 (1994).
14. Berry, F. J., Holden, J. G., and Loretto, M. H., *J. Chem. Soc. Faraday Trans. 1*, **83**, 615 (1987).
15. Muhler, M., Schlögl, R., and Ertl, G., *J. Catal.* **138**, 413 (1992).
16. Wagner, C. D., *Discuss. Faraday Soc.* **60**, 291 (1975).
17. Burriesci, N., Garbassi, F., Peterera, M., and Petrini, G., *J. Chem. Soc. Faraday Trans. 1* **78**, 817 (1982).
18. Allen, M., Betteley, R., Bowker, M., and Hutchings, G. J., *Catal. Today* **9**, 97 (1991).
19. Conner, W. C., and Falconer, J. L., *Chem. Rev.* **95**, 759 (1995).
20. Delmon, B., *Appl. Catal.* **113**, 121 (1994).
21. Weng, L. T., Xiong, Y. L., Ruiz, P., and Delmon, B., *in* "Catalytic Science and Technology" (S. Toshida, N. Takezawa, and T. Ono, Eds.), Vol. 1, p. 207. Kodansha, Tokyo, 1991.
22. Moro-oka, Y., and Ueda, W., *Adv. Catal.* **40**, 233 (1994).
23. Hutchings, G. J., Bowker, M., Crossley, A., Allen, M., and Betteley, R., *Catal. Today* **10**, 413 (1991).
24. Grasselli, R. K., and Suresh, D. D., *J. Catal.* **25**, 273 (1972).
25. Landa-Cánovas, A., Nilsson, J., Hansen, S., Ståhl, K., and Andersson, A., *J. Solid State Chem.* **116**, 369 (1995).
26. Nilsson, R., Lindblad, T., and Andersson, A., *Catal. Lett.* **29**, 409 (1994).
27. Fattore, V., Fuhrman, Z. A., Manara, G., and Notari, B., *J. Catal.* **37**, 215 (1975).
28. Keulks, G. W., Lo, M-Y., *J. Phys. Chem.* **90**, 4768 (1986).